EVIDENCE FOR STRUCTURE IN $\bar{p}p \to \pi^0\pi^0$

R. S. Dulude, R. E. Lanou, Jr., J. T. Massimo, D. C. Peaslee, R. K. Thornton,
Brown University, Providence, Rhode Island 02912 USA.†

D. S. Barton, M. Marx, B. A. Nelson, L. Rosenson,
Massachusetts Institute of Technology, Cambridge, Massachusetts 02139 USA.†

C. DeMarzo, L. Guerriero, F. Posa, E. Vaccari, F. Waldner,
University of Bari and Istituto di Fisica (INFN), Bari 70126 Italy.*

ABSTRACT

We have performed a partial wave amplitude analysis of the angular distributions in the reaction $\bar{p}p \to \pi^0\pi^0$ at 25 energies. The range of center of mass energies covered is from 2.12 to 2.43 GeV and includes the so-called T- and U-meson regions. We find a resonance in the $J^{PC}I^G = 2^{++}0^+$ state in the vicinity of the T (2.15 GeV) and our data are consistent with an additional resonance of $4^{++}0^+$ at the U (2.35 GeV). An isospin decomposition utilizing these data in conjunction with those from $\bar{p}p \to \pi^+\pi^-$ reveals possible difficulties in interpretation.

* * *

We present here the final data sample in an experiment to measure the angular distributions in the reactions $\bar{p}p \to \pi^0\pi^0$ and $\bar{p}p \to \pi^0\eta^0$ in the center of mass interval 2.12 to 2.43 GeV/c^2.

The experiment was performed at the A.G.S. of Brookhaven National Laboratory using an electrostatically separated beam and counter-spark chamber detection techniques. The experimental apparatus, the method of extracting the parent π^0 and η^0 angular distributions from the observed distributions of daughter gamma rays, and some preliminary data have been presented at previous meetings of this symposium series[1] and elsewhere.[2] This final data sample is consistent with the preliminary data set but significantly increases the statistics and includes several more energies for a total of 25 distributions for each reaction, thus making a more complete analysis possible. Figure 1A illustrates the angular distributions for $\bar{p}p \to \pi^0\pi^0$ and Fig. 1B for $\bar{p}p \to \pi^0\eta^0$. The dashed line gives the best estimate of the distribution and the solid curves the allowable range. The data are presented in this way rather than as histograms because, as is discussed in Refs. (1) and (2), the π^0 and η^0 directions are inferred by fitting the distribution derived from their daughter gamma rays directly for the coefficients of a Legendre polynomial expansion of the parent distribution. By this technique we automatically correct for apparatus dependent effects such as gamma ray conversion efficiency and resolution. Several internal consistency checks were made on the method. One such check involved separately fitting to the decidedly different three and four gamma topology data to see if they reconstructed to the same parent angular distribution. The agreement is very good as can be seen for a sample energy in Fig. 2.

In our fits to the data a Legendre expansion up to P_8 was necessary and sufficient to give good fits to the $\bar{p}p \to \pi^0\pi^0$ differential cross sections over the entire energy range. The chi-squared per degree of freedom ranged from 0.2 to 2.4. For the reaction $\bar{p}p \to \pi^0\eta^0$, expansions only up to P_4 were required ($0.2 < \chi^2/DF < 1.8$). Because of the symmetries involved in the two reactions only the even Legendre polynomials are present and thus the angular distributions can be folded about $\cos\theta = 0$. The resulting Legendre coefficients defined by

$$\frac{d\sigma}{d\Omega} = \sum_{\ell(\text{even})}^{\ell_{max}} A_\ell P_\ell(\cos\theta) \qquad (1)$$

are shown in Fig. 3A and Fig. 3B. The reaction cross sections are shown in Figs. 4A and 4B.

The $\pi^0\pi^0$ data has several striking features and we concentrate on that reaction in what follows. The symmetries in this reaction limit the allowed quantum numbers to $J^P = (\text{even})^+$, $I^G = 0^+$, $S_{\bar{p}p} = 1$, $L_{\bar{p}p} = (\text{odd})$ and baryon number zero.

Although this reaction channel represents only a small portion of the total $\bar{p}p$ cross section, recent developments in both theory and experiment emphasize the importance of exclusive channels with restricted sets of quantum numbers. Among the recent developments are: (a) the

†Work supported in part by U.S. Department of Energy under Contracts EY-76-C-02-3069 and -3130.

*Work supported in part by the USA-Italy Scientific Cooperation Program and the Istituto Nazionale di Fisica Nucleare.

(PAPER SUBMITTED TO IV INTERNATIONAL ANTIPROTON SYMPOSIUM -- Strasbourg, France, 26 - 30 June 1978)

DISCLAIMER

interpretation of the T and U structures long present in the total cross section[3] as being built from the J^{PC}, $I^G = (3^{--}, 1^+)$, $(4^{++}; 0^+)$ and $(5^{--}, 1^+)$ resonances seen in $\bar{p}p \to \pi^+\pi^-$,[4] (b) very narrow baryon-antibaryon enhancements observed in production experiments,[5] (c) the development of the concept of baryonium,[6] (d) the possibility of nuclear bound states.[7]

With this in mind we have undertaken an energy-dependent partial wave analysis of $\pi^\circ\pi^\circ$. The model we have used is one in which each partial wave amplitude could be represented as the sum of Breit-Wigner resonances and constant background modified by the appropriate barrier penetration factors. Thus the amplitude for total angular momentum, J, and $L_{\bar{p}p} \equiv L$ is given by

$$a_{JL} = a_{JL}(\text{Resonance}) + b_{JL}(\text{Background}) \tag{2}$$

where

$$a_{JL}(\text{Resonance}) = \sqrt{\frac{\pi\lambda^2 x}{4} T_L(x)}\ \frac{iB_{JL}\Gamma_J}{(E_J - E^*) - i\Gamma_J} \tag{3}$$

$$b_{JL}(\text{Background}) = \sqrt{\frac{\pi\lambda^2 x}{4} T_L(x)}\ [\alpha_{JL} + i\beta_{JL}] \ . \tag{4}$$

It should be noted that only triplet $\bar{p}p$ ($S_{\bar{p}p} = 1$) spin is allowed and that J is constrained to be $J = L \pm 1$. In Eqs. (3) and (4), $x \equiv \frac{p^* R}{\hbar c}$ where the interaction radius R is taken as 1.4 fermi and $T_L(x)$ are the usual barrier penetration factors.[8] B_{JL} is $\sqrt{\gamma_{JL}\gamma_{\pi\pi}/\Gamma^2_J}$ where γ_{JL} is the reduced partial width for the entering channel and $\gamma_{\pi\pi}$ that for the decay channel--B_{JL} is the quantity determined. Γ_J is the full width. The background parameters, α_{JL} and β_{JL}, are constants. In terms of these quantities the differential cross sections can be rewritten as

$$\frac{d\sigma}{d\Omega} = \sum_{J',J} [(\sqrt{J}\, a^*_{J',J-1} - \sqrt{J+1}\, a^*_{J',J+1})(\sqrt{J}\, a_{J,J-1} - \sqrt{J+1}\, a_{J,J+1})] P^\circ_{J'} P^\circ_J$$

$$+ \sum_{J',J} \frac{[(\sqrt{J+1}\, a^*_{J',J-1} + \sqrt{J}\, a^*_{J',J+1})(\sqrt{J+1}\, a_{J,J-1} + \sqrt{J}\, a_{J,J+1})] P^1_{J'} P^1_J}{\sqrt{J'(J+1)(J)(J+1)}} \tag{5}$$

and thus the A_ℓ's of Eq. (1) can be directly related to the a_{JL}'s via the reduction formula for Legendre polynomials.

We use as input to our fitting program the Legendre coefficients of Fig. 3A. Since J must be even and $\ell_{max} = 8$ we allowed for the possibility of resonant states in $J = 0,2,4$ fed from all possible $L_{\bar{p}p}$ values. This model then yields 28 possible parameters to be fitted to a total of 125 data points. Because of the inherent ambiguities of a global fit to the most general version of the model such an approach will not lead simply or directly to a unique solution. Consequently, we have adopted a more piecewise approach based upon the more striking features of the data (e.g., the large negative excursion in A_6 centered at 2.18 GeV) and the inclusion of resonances to be expected from other data already in the literature.[4,9] While this procedure is not exhaustive it does produce a minimal set of solutions and eliminates several possibilities.

Six classes of fits were obtained which described the data and are summarized in Table 1. The results of Fit #3 are typical and appear as solid curves in Fig. 3A. A general feature of the first five of these fits is the presence of a strong $J^P I^G = 2^+0^+$ resonance. The first four fits are similar in that they all have about the same value for the mass and width of this state ($M = 2.15$ GeV/c^2, $\Gamma = 0.25$ GeV). The fifth fit is significantly different in that $M = 2.05$ GeV/c^2. The sixth fit is the best result obtained without including a $J = 2$ resonance.

Fits #3, #4 and #5 contain as one common feature the inclusion of a $J^P = 4^+$ at a mass whose central value is just below our energy range. It is the h-meson[9] and its position and total width were fixed and only its partial widths varied. Although the h-meson's coupling to $\bar{p}p$ is unknown, its quantum numbers and large branching into $\pi^\circ\pi^\circ$ make it a logical candidate for inclusion in the class of fits attempted. Fit #5 had in addition a fixed mass and width $J = 2$ resonance at 2.05 GeV/c^2 and 0.20 GeV, respectively. All of these fits contained JL = OP, 2P, 2F, 4F, and 4H background terms.

In our choice of starting values for each fit we were guided by grid searches in parameter space which identified important partial waves. The usual case was that a range of starting values produced the same fitted result, or, outside that range, no acceptable fit was achieved.

The best fits all required the inclusion of a 2^+ resonance. Our best attempt at fitting with $\pi^\circ\pi^\circ$ 2^+ is listed as Fit #6 in Table 1, and is shown in Fig. 5. The necessity for this state derives from the strong energy dependencies of A_2 and A_6. To illustrate this, consider

first the following expansions of A_6 and A_8 in terms of their partial wave amplitudes.

$$A_6 = .758|a_{4F}|^2 + .970|a_{4H}|^2$$
$$+ 2\mathrm{Re}(-2.624a^*_{2F}a_{4F} - 2.587a^*_{2P}a_{4H} + .822a^*_{2F}a_{4H} - .949a^*_{4F}a_{4H}) \quad (6)$$

$$A_8 = .685|a_{4H}|^2 + 2\mathrm{Re}(-3.065a^*_{4F}a_{4H}) \quad (7)$$

If we eliminate the term proportional to $\mathrm{Re}(a^*_{4F}a_{4H})$ between (6) and (7) we arrive at the linear combination

$$T = A_6 - \left(\frac{.949}{3.065}\right)A_8 = A_6 - .310A_8 = .758|a_{4F}|^2 + .758|a_{4H}|^2$$
$$+ 2\mathrm{Re}(-2.624a^*_{2F}a_{4F} - 2.587a^*_{2P}a_{4H} + 0.822a^*_{2F}a_{4H}) \quad (8)$$

which has as its non-positive definite part only terms involving J = 2,4 interference. Since experimentally A_6 is negative (or very small) over its range and A_8 is mainly positive we have T quite negative over the whole range. Such behavior can only arise if there is a large component of J = 2, J = 4 interference.

If we now turn to A_2 we notice that it has a rapid variation with energy. It is the presence of the sign-changing dip in A_2 at $\sqrt{s}$ = 2.25 GeV together with the large negative dip in A_6 that requires the 2^+ contribution to be strongly energy dependent. The strength of the J = 4 that can be included is bounded in the low energy region by the smallness of A_8 and in the high energy region by A_0; in neither case are we permitted a very large contribution to the interference from a high mass resonance in J = 4. This has bearing on the $J^PI^G = 4^+0^+$ resonance deduced in Ref. (4); we discuss this further below.

While we cannot distinguish between Fits 01 and 05 on the basis of χ^2 we can argue preferences on the basis of comparison with data from the related reaction, $\bar{p}p \to \pi^+\pi^-$.[4] The energy range of Ref. (4) is somewhat larger than ours, extending slightly beyond our range at both ends.

The $\pi^+\pi^-$ final state is comprised of both I = 0 and I = 1 contributions. For the iso-spin cross sections we have

$$\sigma(I = 0) = 3\sigma(\pi^0\pi^0)$$
$$\sigma(I = 1) = \sigma(\pi^+\pi^-) - 2\sigma(\pi^0\pi^0)$$

while the differential cross sections [if $M(\pi^+\pi^-) \equiv M(I = 0) + M(I = 1)$ and $M(\pi^0\pi^0) \equiv M(I = 0)$] are given by

$$\frac{d\sigma(\pi^0\pi^0)}{d\Omega}(\theta) = |M_0|^2 = \sum_{\ell\,\mathrm{even}} A^0_\ell P_\ell(\theta) \quad (10)$$

$$\frac{d\sigma(\pi^+\pi^-)}{d\Omega}(\theta) = |M_0|^2 + |M_1|^2 + 2\mathrm{Re}\, M_0M_1$$
$$= \sum_{\ell\,\mathrm{even}} A^0_\ell P_\ell(\theta) + \sum_{\ell\,\mathrm{even}} A^1_\ell P_\ell(\theta) + \sum_{\ell\,\mathrm{odd}} A^{01}_\ell P_\ell(\theta) \quad (11)$$

where A^I_ℓ denotes the various isospin contributions to the ℓ^{th} partial wave. Hence subtraction of the angular distributions for the two reactions illustrates that the A^0_ℓ and A^1_ℓ coefficients can be directly extracted from the data without appeal to any fitted models.

$$\frac{d\sigma(\pi^+\pi^-)}{d\Omega} - \frac{d\sigma(\pi^0\pi^0)}{d\Omega} = \sum_{\ell\,\mathrm{even}} A^1_\ell P_\ell(\theta) + \sum_{\ell\,\mathrm{odd}} A^{01}_\ell P_\ell(\theta) \quad (12)$$

We have performed this subtraction using the even coefficients and the I = 0 and I = 1 coefficients are given respectively in Figs. 3A and 6. Since the energies at which Ref. (4) data points were taken are not exactly the same as ours we have interpolated their coefficients. The cross sections for (I = 0) and (I = 1) are given by the points in Figs. 7A and 7B. It is important to note that our experiment neasured I = 0 only and that the separation indicated by the points is model independent. In an analysis solely internal to the $\pi^+\pi^-$ data, the authors of Ref. (4) have found the contributions from the various partial waves in both I = 0 and I = 1 (see Fig. 8). Using these fits[10] we have generated what their analysis would give for $\sigma(I = 0)$ and $\sigma(I = 1)$; these are plotted as solid curves in Figs. 7A and 7B. There are clear inconsistencies. In particular: (a) For I = 0, our data have a larger contribution in the vicinity of 2150 MeV and a smaller one near 2320 MeV than does Ref. (4), while (b) for the I = 1 the reverse is true. It is interesting to note that the locations of the resonances found by the authors of Ref. (4) are $J^PI^G(\mathrm{MASS}) = 3^-1^+$ (2150), 4^+0^+ (2310), 5^-1^+ (2480). Table 2 contains these parameters from Ref. (4).

The solutions of Ref. (4) can also be used to generate predicted angular distributions for $\pi^0\pi^0$ in our energy region. The authors of Ref. (4) have kindly provided us with such distributions. Figure 9 illustrates a comparison with their predictions and our measurements

at several energies. The disagreement consists chiefly of a failure to predict a strong forward dip in the energy range 2.1-2.3 GeV. The presence of this strong forward dip can be traced directly to the J = 2,4 interference and its absence in the predicted distribution is no doubt due to the lack of a strong J = 2 wave.

How do our resonance fits impinge on these discrepancies and can a combination of the two independent analyses be used to favor any of the fits?

(a) Fits #4 and #5: If we use our Fit #5 (or #4) to extend into the lower end of the Ref. (4) energy range (see Fig. 10) we find that I = 0 accounts for virtually all of the $\pi^+\pi^-$ cross section below about 2.1 GeV. This is clearly unacceptable if there is any significant J = 3 in I = 1. It should be noted that $\sigma(I = 1)/\sigma(I = 0) \gtrsim 3$ elsewhere. Since the evidence for J = 3 seems quite strong we consider Fit #5 (and #4) as unlikely.

(b) Fits #1 and #2 (see Fig. 11): These two fits test the need for a J = 4 (M = 2330) resonance. We can obtain a fit without this resonance (i.e., Fit #2), but if we include it the resulting parameters for the resonance are in agreement with Ref. (4). Note that we require smaller reduced partial widths and the data does not permit its production at a level large enough (by about a factor 4) to account for the A_6 structure by a J = 4 (M = 2330) resonance interfering with a J = 2 background.

(c) Fit #3 (see Fig. 3A): This fit differs principally from #1 and #2 in its inclusion of the h-meson. As such it provides an estimate of the upper limit to the coupling the h-meson can have to $\bar{p}p$. Note that all three fits give the same J = 2 and J = 4 parameters.

We draw the following conclusions from this comparison:

(1) Our data requires a $J^PI^G = 2^+0^+$; the parameters of the preferred solution are M = 2.150 GeV/c^2, Γ = 0.25 GeV. This new resonance can be interpreted as the I = 0 contribution to the T region making an isospin doublet of the T as is known to be the case for the S and U.

(2) A resonance in $J^PI^G(M,\Gamma) = 4^+0^+(2330,0.3)$ is consistent with but not required by our data.

(3) It seems likely that an analysis of the combined $\pi^\circ\pi^\circ$ and $\pi^+\pi^-$ data will resolve the discrepancy in the I = 0, I = 1 separation and probably produce the same set of resonances in J = 2,3,4, and 5 but with different strengths than we now understand them to have. At least one such analysis is underway[11] and hopefully before the next of these Symposia we will know the result.

As to interpretation of these results in terms of different models[6] we are not prepared to draw a definite conclusion. We would note, however, that their rather broad widths do not exclude an interpretation as nuclear states;[7] on the other hand the new $J^PI^G = 2^+0^+$ resonance when placed on a Chew-Frautschi plot falls near the M_2^J and M_0^J trajectories of Rossi and Veneziano (see Fig. 13).

Finally a comment on the $\bar{p}p \to \pi^\circ\eta^\circ$ data. The lower level of activity in these coefficients does not warrant an equivalent analysis at the present time. The most exceptional characteristic of this data is the large and constant A_4/A_0 over the entire energy range. This might be due to a large $J^{PC}I^G = 2^{++}1^-$, as has been pointed out.[12] If this is true it might be related to the broad enhancements into $2\pi^+2\pi^-\pi^\circ$ and $K_s^0K^\pm\pi^\mp$ centered at ∿ 2000 MeV with width ∿ 100 MeV seen in other $\bar{p}p$ experiments.[13]

We wish to thank the Brookhaven National Laboratory for their hospitality and technical support. We especially want to acknowledge the invaluable aid we received from T. F. Lyons, E. Druek, G. Krey, S. Redner, J. Butler and G. C. Y. Chen. Finally we also wish to thank the scanning staffs at our respective institutions for their outstanding efforts.

REFERENCES

1. C. DeMarzo, et al., Proceedings of II International Antiproton Symposium, Libbice-Prague, CERN 74-18 (1974); C. DeMarzo, et al., Proceedings of III Antiproton Symposium, Stockholm, Pergamon Press (Oxford) 1977.

2. M. D. Marx, M.I.T. Ph.D. Thesis (unpublished) 1974; R. K. Thornton, Brown University Ph.D. Thesis (unpublished) and Internal Report #136

(COO-3130 TB-220) 1976; C. DeMarzo, et al., Nucl. Instr. Methods 131 (1975) 47.

3. R. J. Abrams, et al., Phys. Rev. D1 (1970) 1917; J. Alspector, Phys. Rev. Letts. 30 (1973) 51; D. C. Peaslee, et al., Phys. Letts. 57B (1975) 189.

4. E. Eisenhandler, et al., Nucl. Phys. 113B (1976), 1; A. A. Carter, et al., Phys. Letts. 67B (1977) 117: A. A. Carter, et al., Phys. Letts. 67B (1977) 122.

5. P. Benkheiri, et al., Phys. Letts. 68B (1977), 483; C. Evangelista, et al., Phys. Letts. 72B (1977) 139; A. Apostolakis, et al., Phys. Letts. 66B, No. 2, (1977), 185.

6. G. F. Chew in Proceedings of III International Antinucleon Symposium, Stockholm (1976) Pergamon Press, p. 515; H. I. Miettenen, ibid, p. 495; G. C. Rossi and G. Veneziano, CERN pre-print THY2287 (unpublished) 1977 and Nucl. Phys. B123 (1977) 507; Chan, H-M., et al., Phys. Letts. 72B (1978) 400; Chan, H-M. and H. Hogaasen, Phys. Letts. 58B (1975) 93; M. Fukugita, et al., Phys. Letts. 74B deGrand, et al., Phys. Rev. D12 (1975) 37.

7. L. N. Bogdanova, et al., Ann. Phys. 84 (1974) 261; C. B. Dover, Proc. of Syracuse Conference. Vol. II (1975) 37; A. Kerman, private communication.

8. J. M. Blatt and V. Weisskopf, Theoretical Nuclear Physics (John Wiley) p. 358 (1952).

9. W. D. Apel, et al., Phys. Letts. 57B (1975) 398; W. Blum, et al., Phys. Letts. 57B (1975), 403.

10. We are indebted to E. Eisenhandler for providing us with these pre-publication data.

11. Private communication from R. J. Kelly and J. Alcock.

12. L. Montanet, Proceedings V International Conference on Experimental Meson Spectroscopy (editors, von Goeler and Weinstein). Northeastern Univ. Press (1977).

13. C. Defoix, et al., College de France. Pre-print ØLPC 75-04 (unpublished) and quoted in Ref. 12.

FIGURE CAPTIONS

Fig. 1A: Angular distributions of $\bar{p}p \to \pi^\circ\pi^\circ$.

Fig. 1B: Angular distributions of $\bar{p}p \to \pi^\circ\eta^\circ$.

Fig. 2: Parent $\pi^\circ\pi^\circ$ distributions from 3 and 4 gamma ray topologies at $P_{lab} = 1.838$ GeV/c. Error bars are shown at points of worst agreement. The histogram is the observed 3 and 4 gamma data sample.

Fig. 3A: Legendre coefficients A_L for $\pi^\circ\pi^\circ$ (solid curve is for Fit Ø3).

Fig. 3B: Legendre coefficients for $\pi^\circ\eta^\circ$.

Fig. 4A: Cross section for $\pi^\circ\pi^\circ$.

Fig. 4B: Cross section for $\pi^\circ\eta^\circ$.

Fig. 5: Fit Ø6 extended to include energy region of Ref. (4) (data points are the same as Fig. 3A).

Fig. 6: Legendre coefficients for $I = 1^+$.

Fig. 7A: Cross section in $I = 0$. Points are those of this experiment; curve is from Ref. (4) analysis.

Fig. 7B: Cross section in $I = 1$. Points are those found in subtraction of $\pi^\circ\pi^\circ$ and $\pi^+\pi^-$ data; curve is from Ref. (4) analysis. (Note different scale.)

Fig. 8: Partial wave contributions to $\pi^+\pi^-$ as determined in Ref. (4).

Fig. 9: Comparison of selected $\pi^\circ\pi^\circ$ distributions. Solid curves are from this experiment, dashed ones are deduced from Ref. (4).

Fig. 10: Extended fits for Fit Ø5. Points are same as Fig. 3A.

Fig. 11: Extended fits for Fit Ø2. Points are same as Fig. 3A.

Fig. 12A: Partial wave contributions to $\pi^\circ\pi^\circ$ from this analysis (Fit Ø1).

Fig. 12B: Partial wave contributions to $\pi^\circ\pi^\circ$ from this analysis (Fit Ø3).

Fig. 13: Chew-Frautschi plot. Crosses are for $J = 2$ and $J = 4$ of this analysis. M_I^J trajectories are from Rossi and Vineziano (Ref. 6).

Table I (This experiment)

Fit #	$J^P = 2^+$ MASS†	Γ_2†	B_{2P}	B_{2F}	$J^P = 4^+$ (lower) MASS	Γ_4	B_{4F}	B_{4H}	$J^P = 4^+$ (upper) MASS	Γ_4	B_{4F}	B_{4H}	χ^2	χ^2/DF
1	2.16	.25	-.02	.08	-	-	-	-	2.33	.25	.008	-.005	219	2.05
2	2.13	.24	-.02	.10	-	-	-	-	-	-	-	-	227	2.01
3	2.15	.26	-.01	.08	2.02*.18*		.03	.02	2.33	.22	.008	-.005	232	2.21
4	2.15	.12	-.006	.07	2.02*.18*		.09	-.01	2.32	.17	-.014	.006	236	2.25
5	2.05*	.20*	-.10	.07	2.02*.20*		-.05	-.01	2.35	.21	-.004	.02	260	2.41
6	-	-	-	-	2.02*.18*		.10	-.008	2.34	.20	-.011	.006	351	3.22

* = Parameter held fixed

† = Units are in GeV/c^2 and GeV respectively; errors on M and Γ_J are ± .01 and on B_{JL} are ± .005.

Note: Copies of tables of the Legendre coefficients and the associated error matrix are available by writing to one of the authors (R. S. Dulude).

Table II (Data from Ref. (4))

J	MASS(MeV/c^2)	Γ(MeV)	Phase	Y_{++}	Y_{+-}
3	2150	200	0	-.073	.153
4	2310	210	-.85	-.083	.043
5	2480	280	2.36	.035	-.068

Note: Ref. (4) Breit-Wigner parameterization $f_{+\pm} = \dfrac{e^{i\phi_J} Y_{+\pm} \Gamma\sqrt{s_0}}{(s - s_0) + i\Gamma\sqrt{s_0}}$

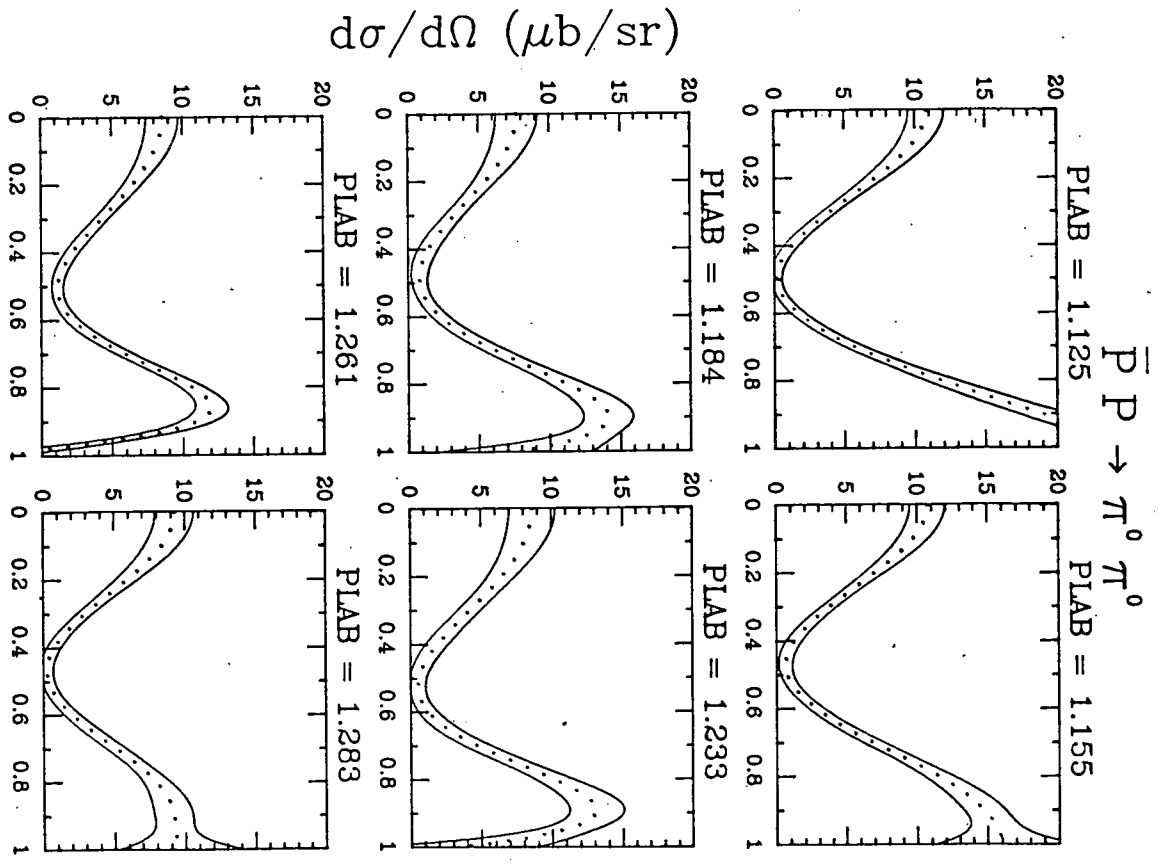

Fig. 1A

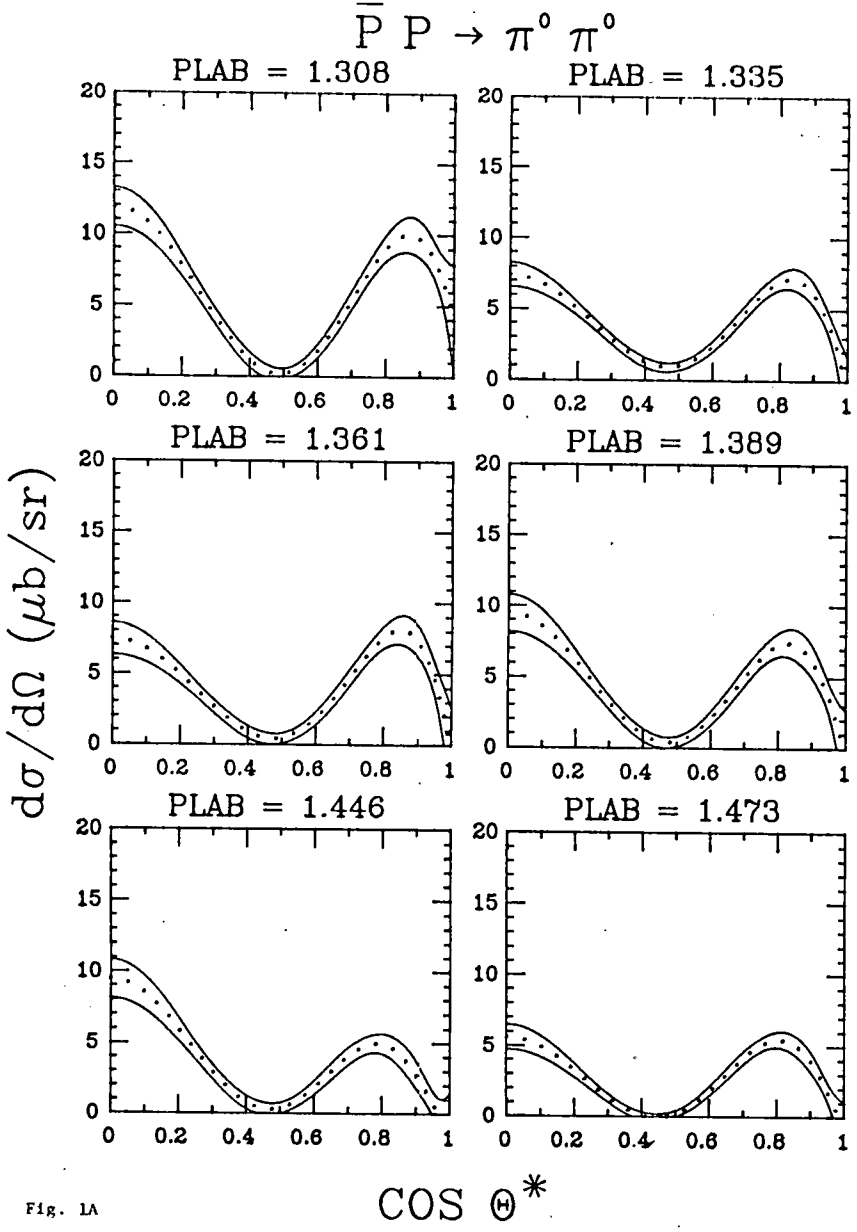
$\bar{P}\,P \rightarrow \pi^0\,\pi^0$
PLAB = 1.308
PLAB = 1.335
PLAB = 1.361
PLAB = 1.389
PLAB = 1.446
PLAB = 1.473
$d\sigma/d\Omega$ (μb/sr)
COS Θ^*

Fig. 1A

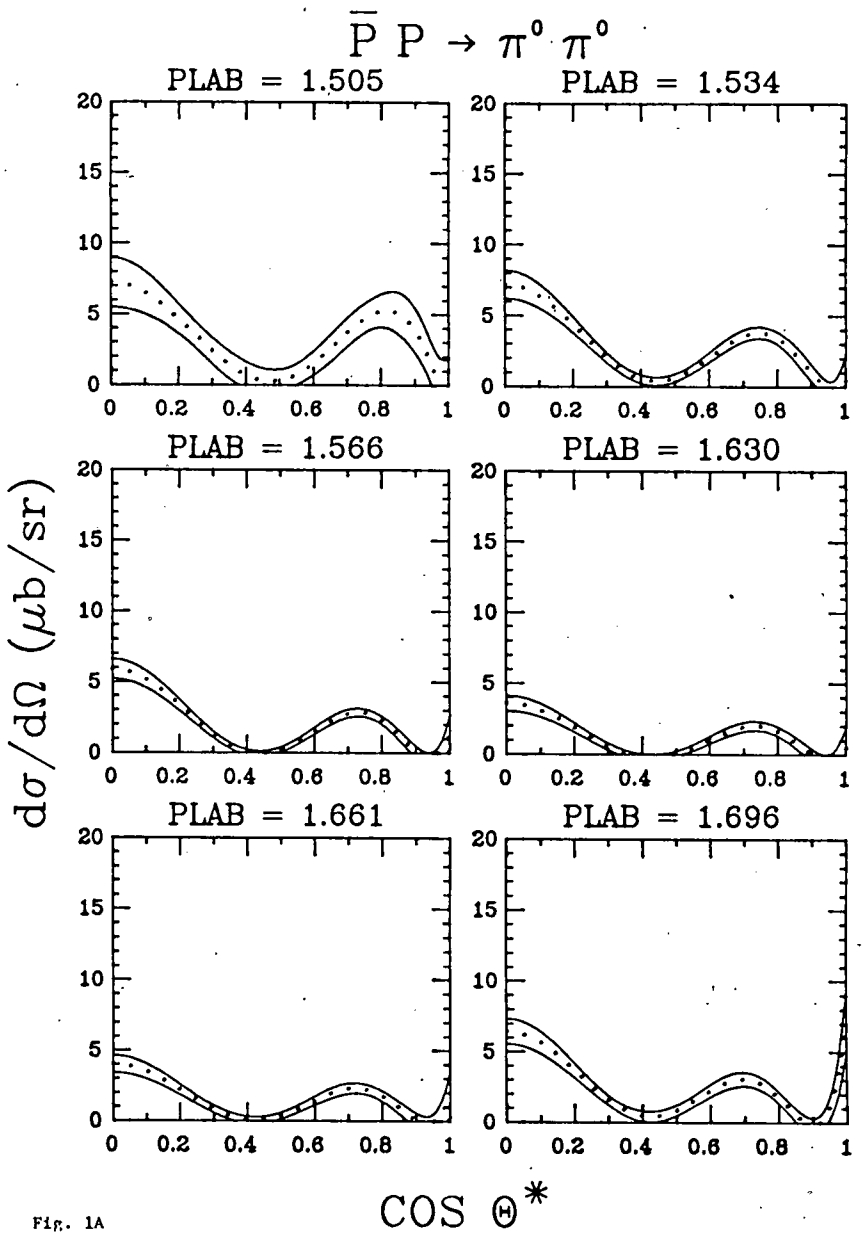
$\bar{P}\,P \rightarrow \pi^0\,\pi^0$
PLAB = 1.505
PLAB = 1.534
PLAB = 1.566
PLAB = 1.630
PLAB = 1.661
PLAB = 1.696
$d\sigma/d\Omega$ (μb/sr)
COS Θ^*

Fig. 1A

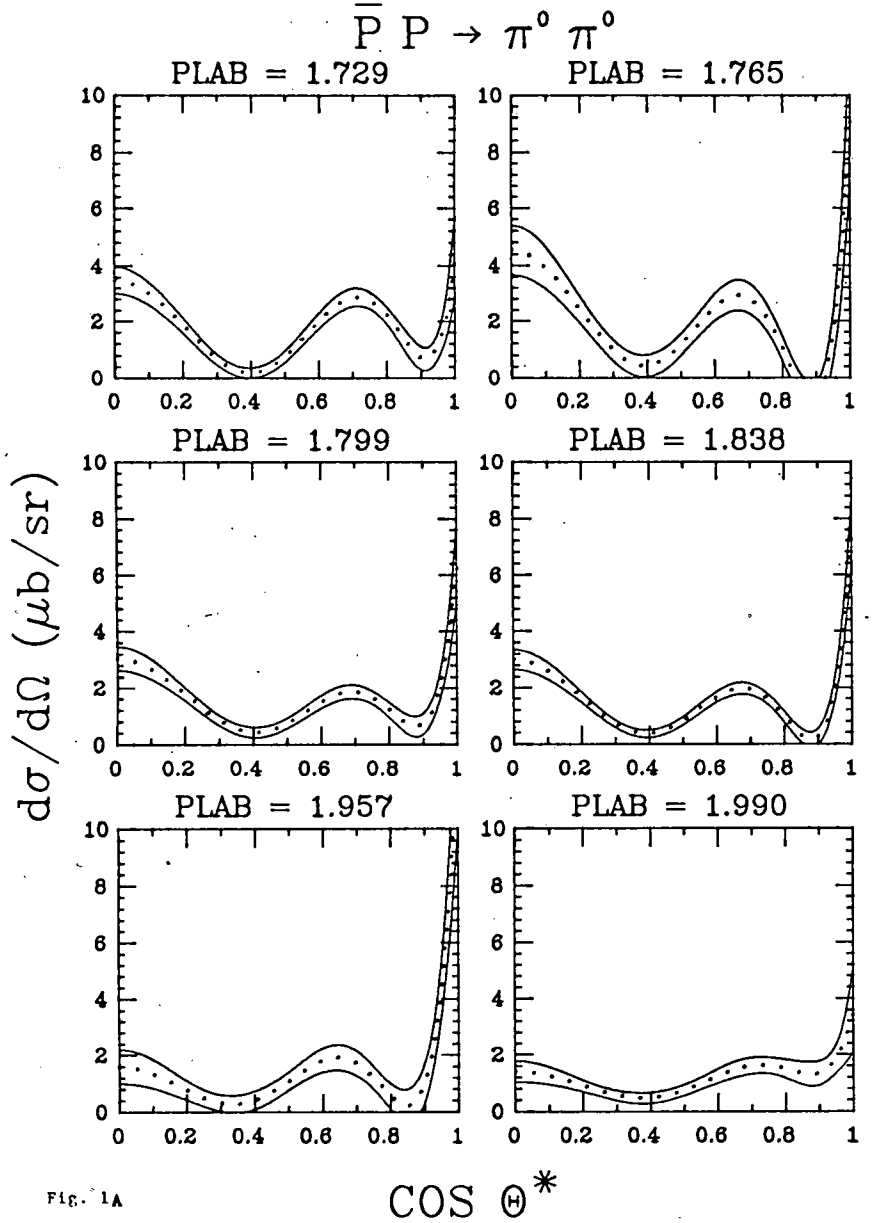
$\bar{P}\,P \rightarrow \pi^0\,\pi^0$
PLAB = 1.729
PLAB = 1.765
PLAB = 1.799
PLAB = 1.838
PLAB = 1.957
PLAB = 1.990
$d\sigma/d\Omega$ (μb/sr)
COS Θ^*

Fig. 1A

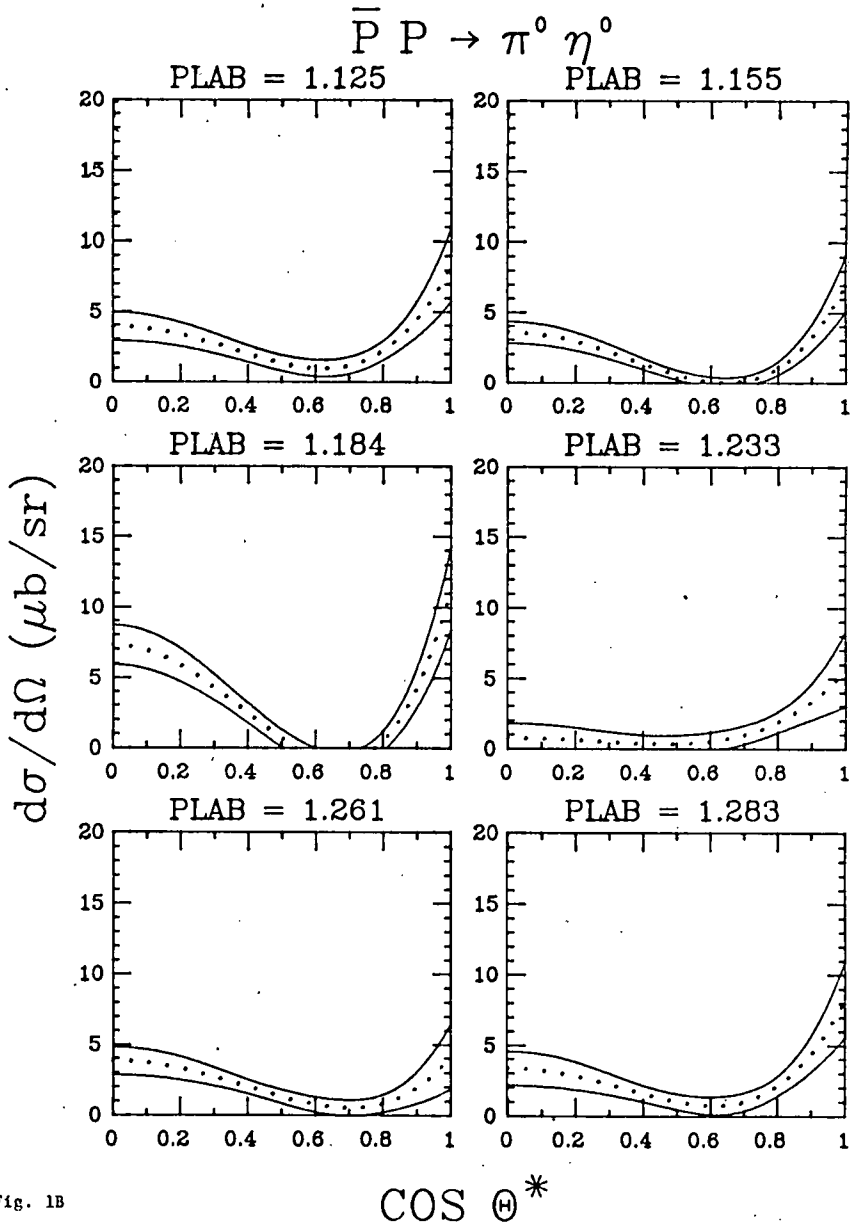
$\bar{P}\,P \rightarrow \pi^0\,\eta^0$
PLAB = 1.125
PLAB = 1.155
PLAB = 1.184
PLAB = 1.233
PLAB = 1.261
PLAB = 1.283
$d\sigma/d\Omega$ (μb/sr)
COS Θ^*

Fig. 1B

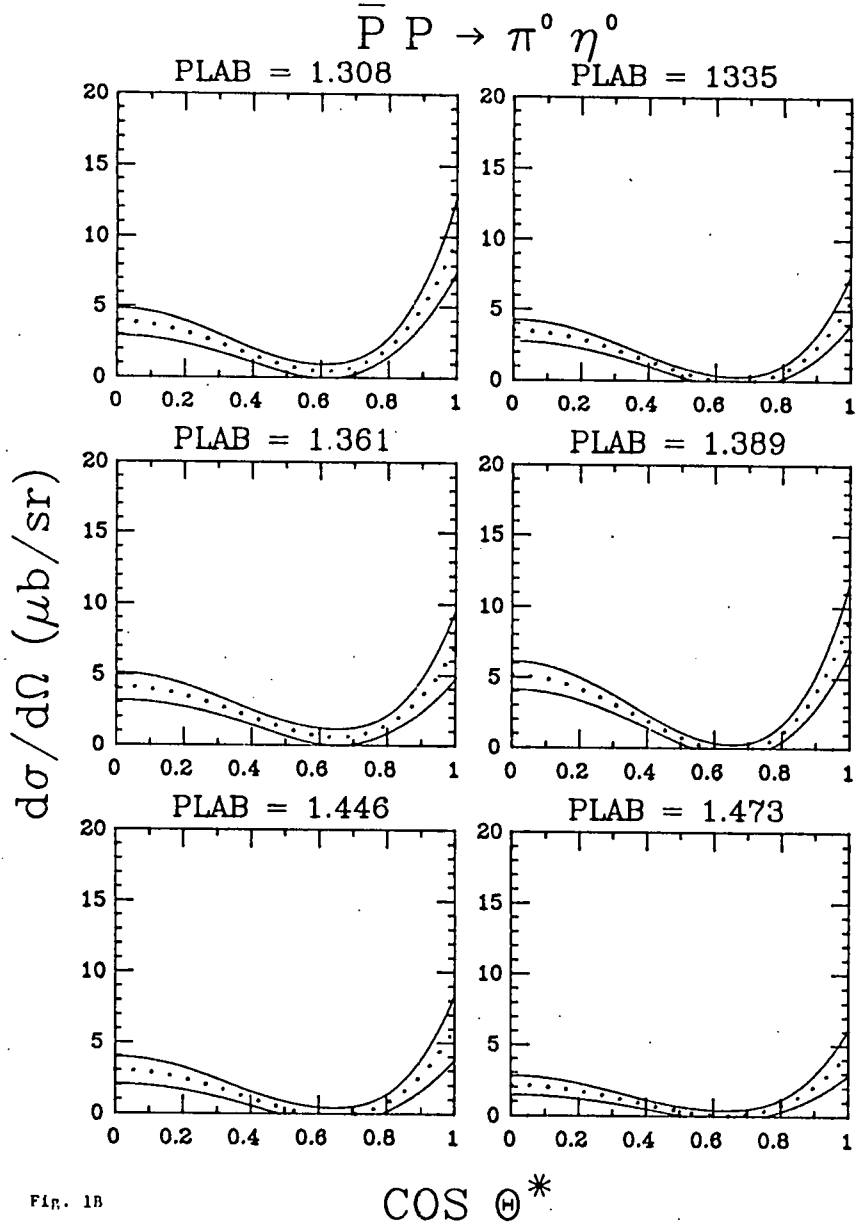
$\bar{P}\,P \rightarrow \pi^0\,\eta^0$
PLAB = 1.308
PLAB = 1335
PLAB = 1.361
PLAB = 1.389
PLAB = 1.446
PLAB = 1.473
$d\sigma/d\Omega$ (μb/sr)
COS Θ^*

Fig. 1B

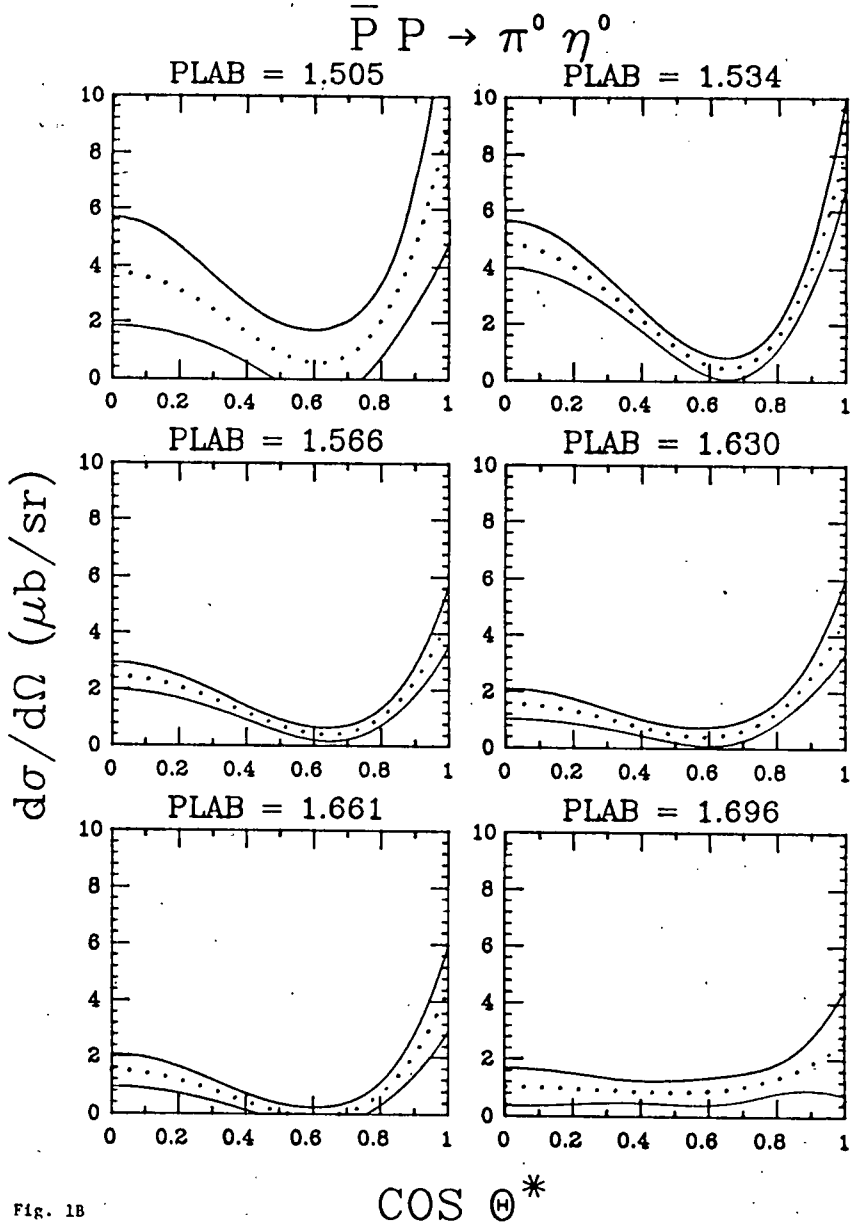
$\bar{P}\,P \rightarrow \pi^0\,\eta^0$
PLAB = 1.505
PLAB = 1.534
PLAB = 1.566
PLAB = 1.630
PLAB = 1.661
PLAB = 1.696
$d\sigma/d\Omega$ (μb/sr)
COS Θ^*

Fig. 1B

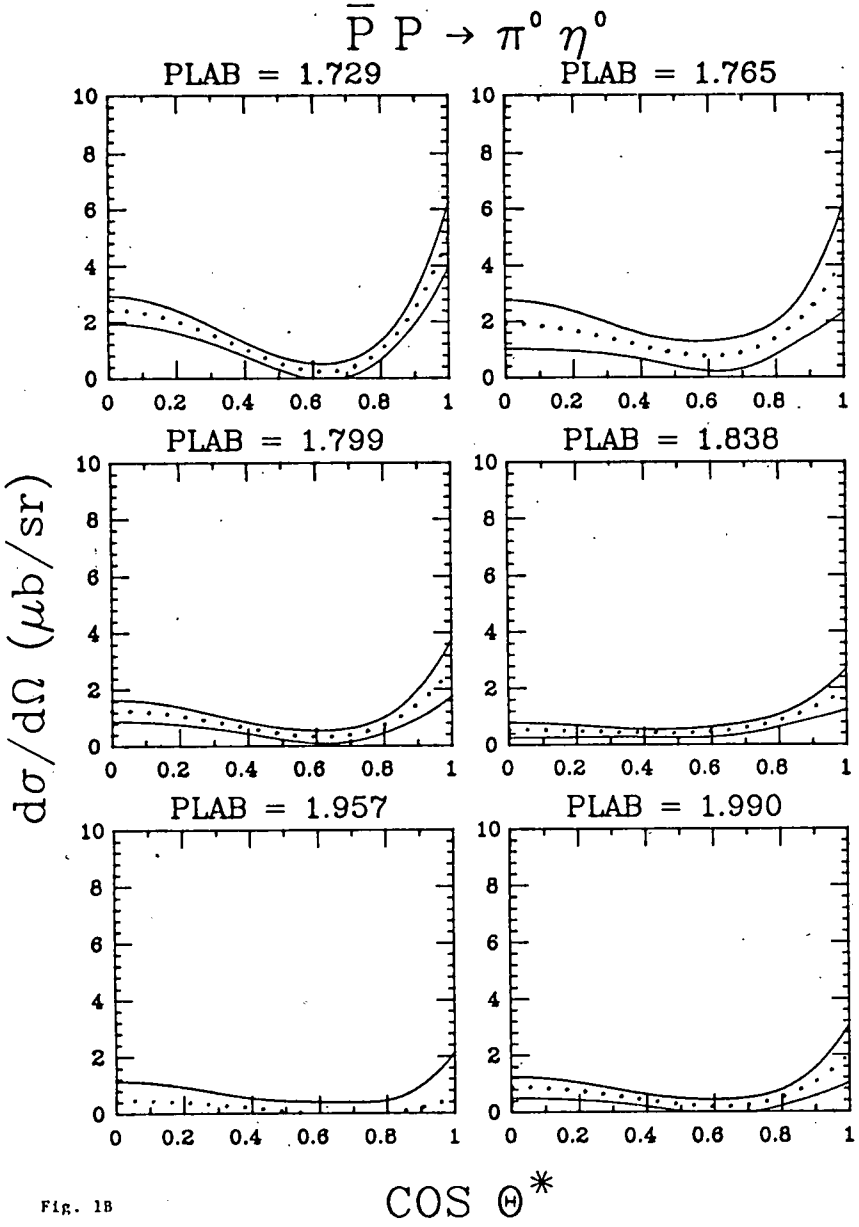
$\bar{P}\,P \rightarrow \pi^0\,\eta^0$
PLAB = 1.729
PLAB = 1.765
PLAB = 1.799
PLAB = 1.838
PLAB = 1.957
PLAB = 1.990
$d\sigma/d\Omega\ (\mu b/sr)$
COS Θ^*

Fig. 1B

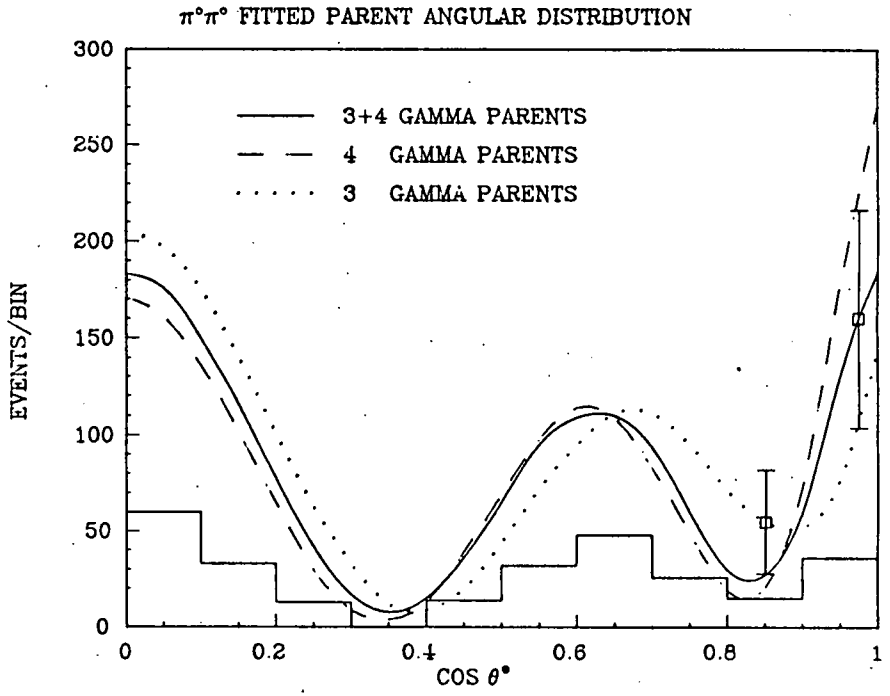
$\pi^\circ\pi^\circ$ FITTED PARENT ANGULAR DISTRIBUTION
3+4 GAMMA PARENTS
4 GAMMA PARENTS
3 GAMMA PARENTS
EVENTS/BIN
COS θ^*

Fig. 2

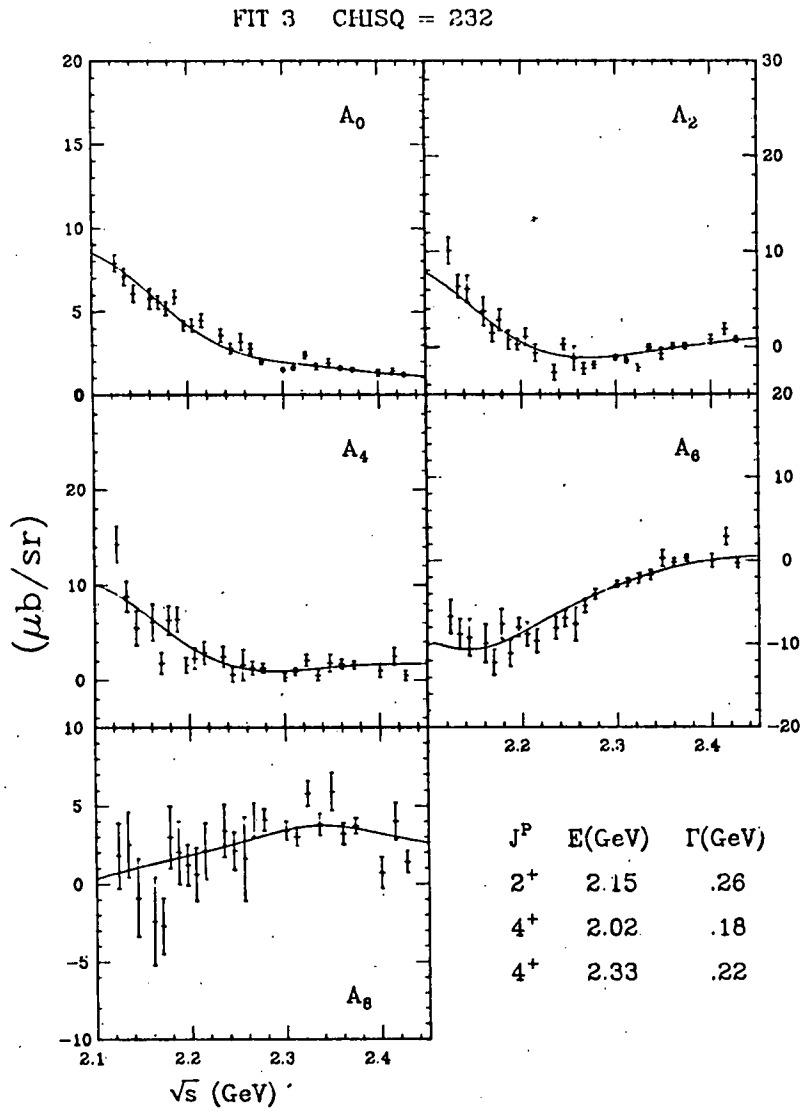
FIT 3 CHISQ = 232
A_0
A_2
A_4
A_6
A_8
$(\mu b/sr)$
$\sqrt{s}$ (GeV)
J^P E(GeV) Γ(GeV)
2^+ 2.15 .26
4^+ 2.02 .18
4^+ 2.33 .22

Fig. 3A

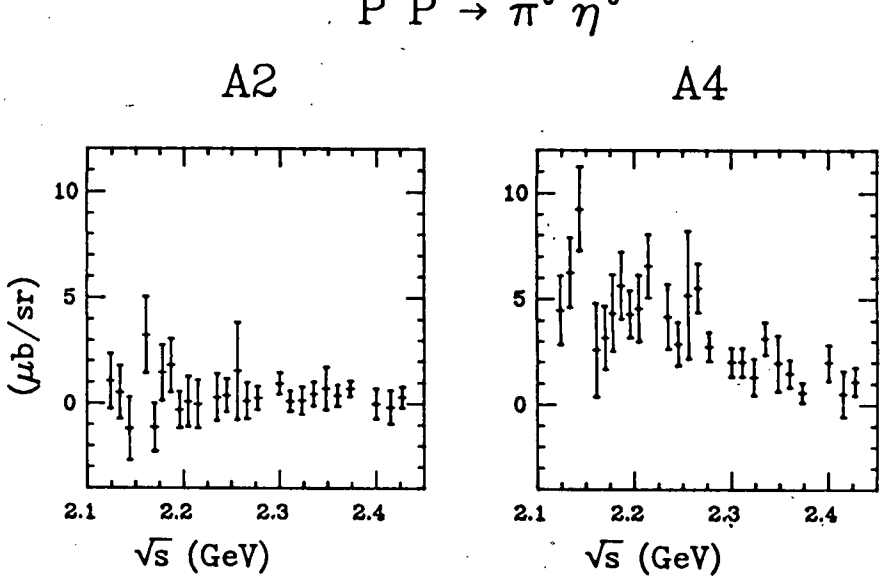
$\overline{P}\,P \rightarrow \pi^0\,\eta^0$
A2
A4
$(\mu b/sr)$
$\sqrt{s}$ (GeV)
$\sqrt{s}$ (GeV)

Fig. 3B

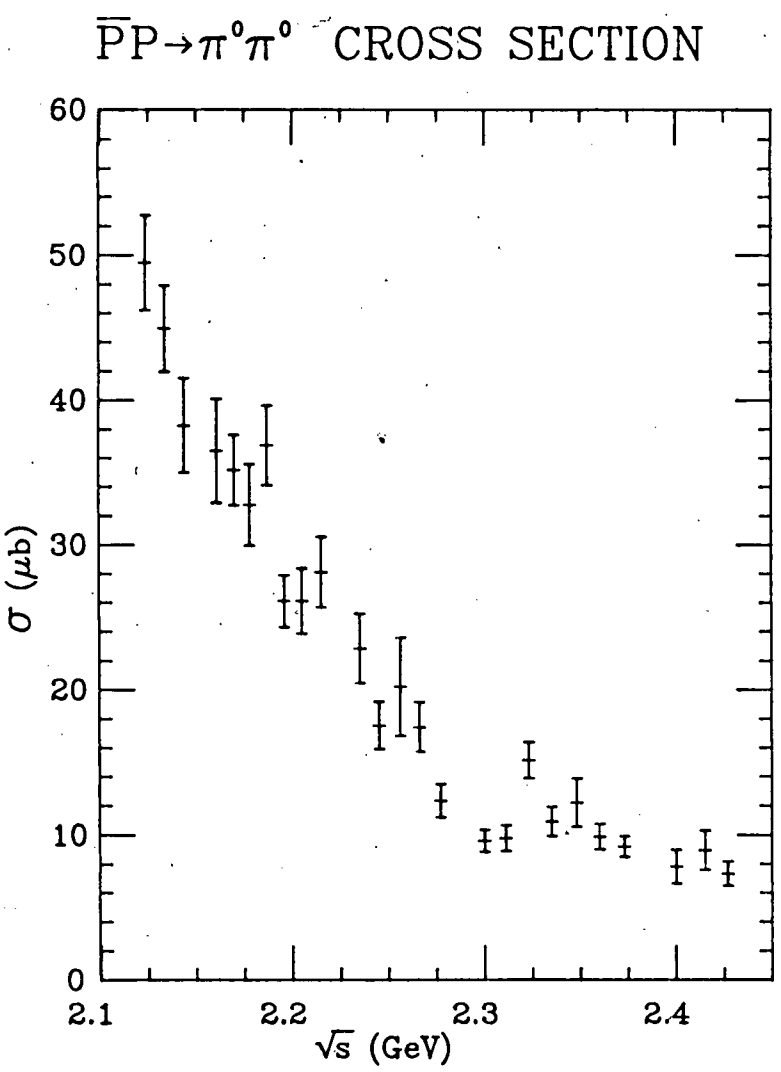
$\bar{P}P \to \pi^0\pi^0$ CROSS SECTION
60
50
40
30
20
10
0
σ (μb)
2.1
2.2
2.3
2.4
$\sqrt{s}$ (GeV)

Fig. 4A

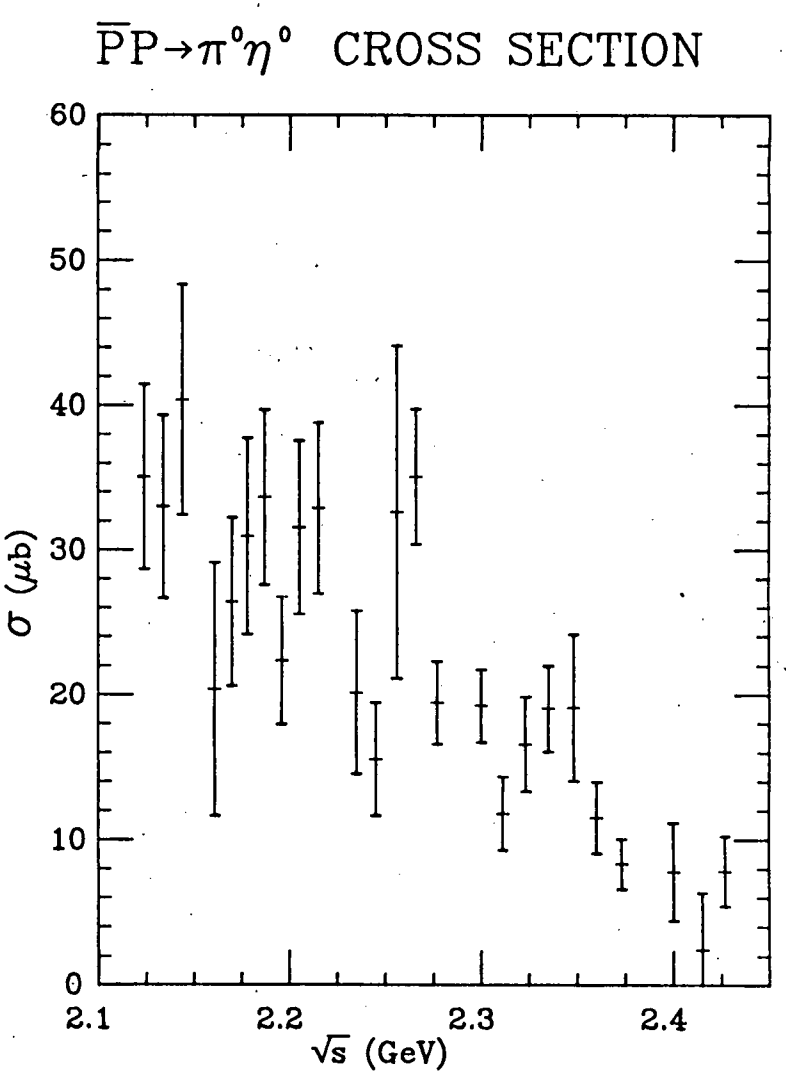
$\bar{P}P \to \pi^0\eta^0$ CROSS SECTION
60
50
40
30
20
10
0
σ (μb)
2.1
2.2
2.3
2.4
$\sqrt{s}$ (GeV)

Fig. 4B

FIT 6 CHISQ = 351

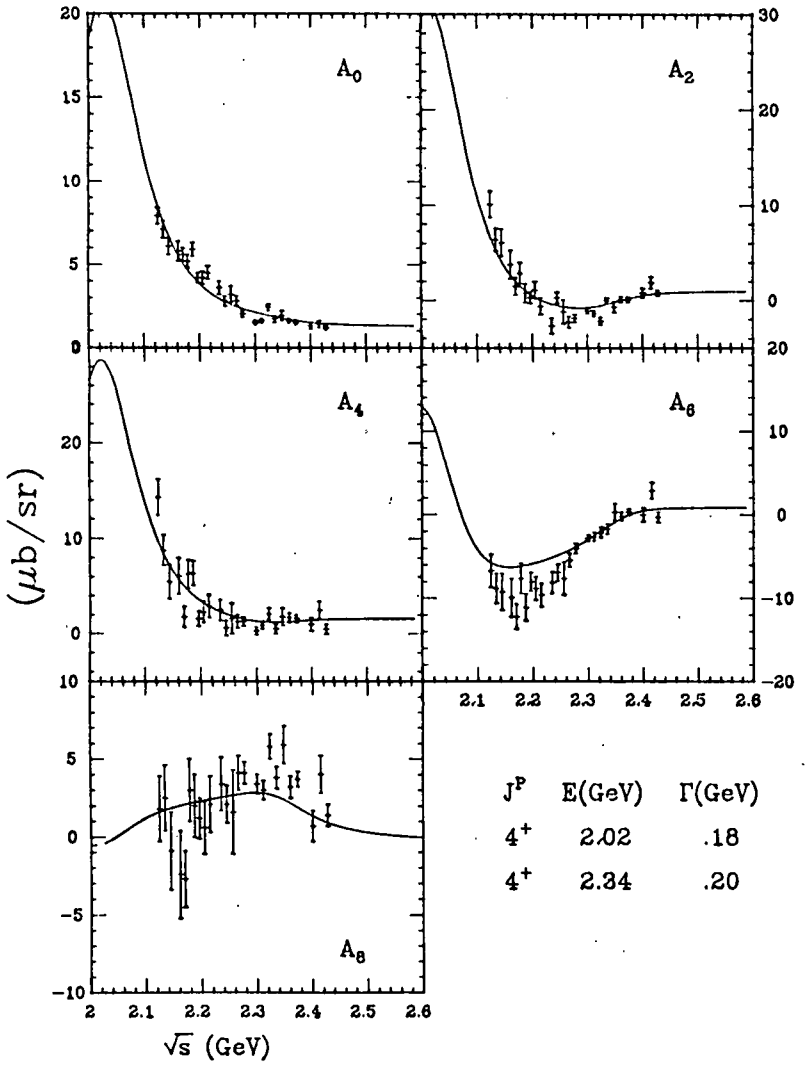

J^P	E(GeV)	Γ(GeV)
4^+	2.02	.18
4^+	2.34	.20

Fig. 5

ISOSPIN 1^+

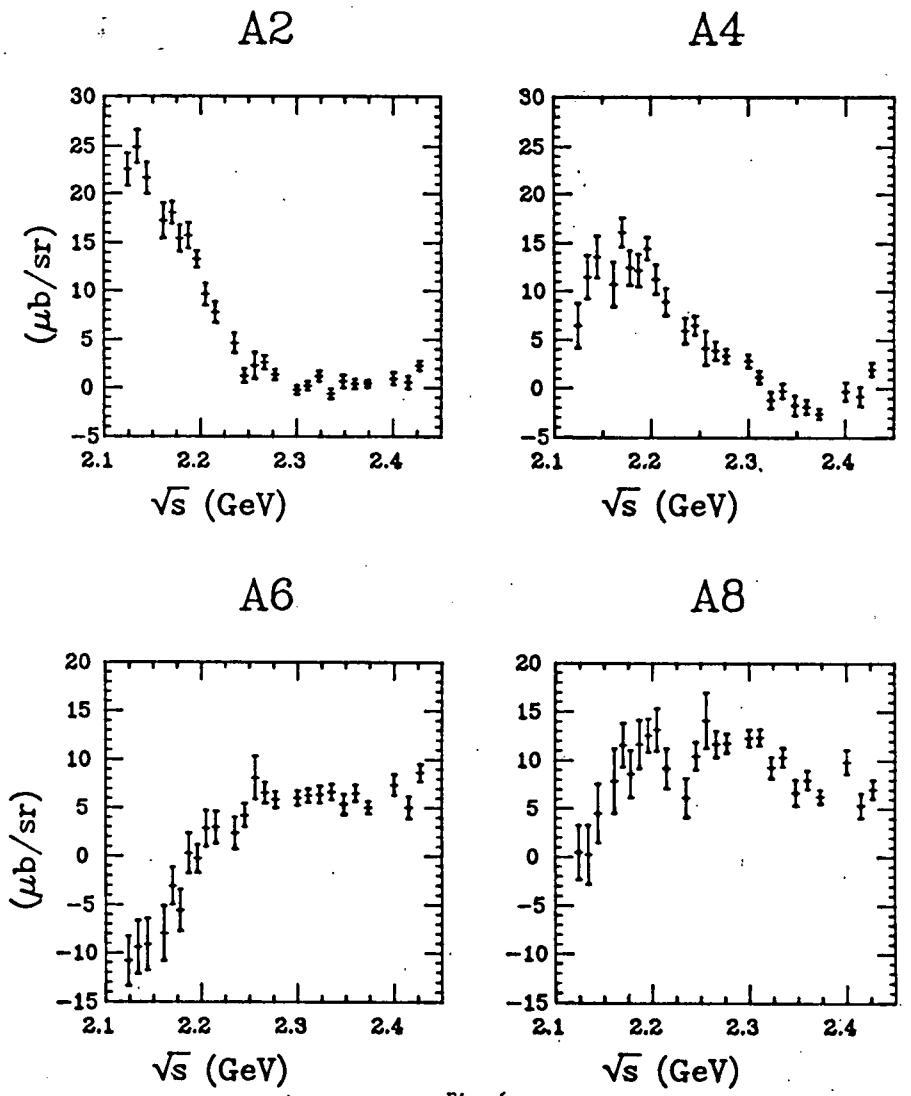

Fig. 6

ISOSPIN SEPARATION

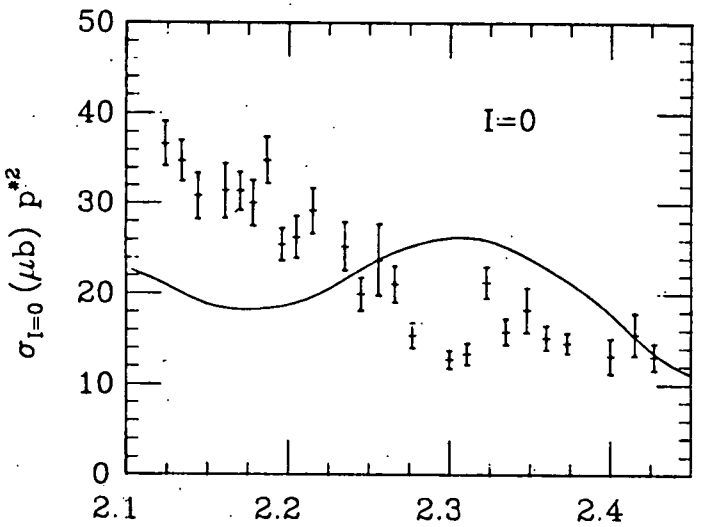

Fig. 7A

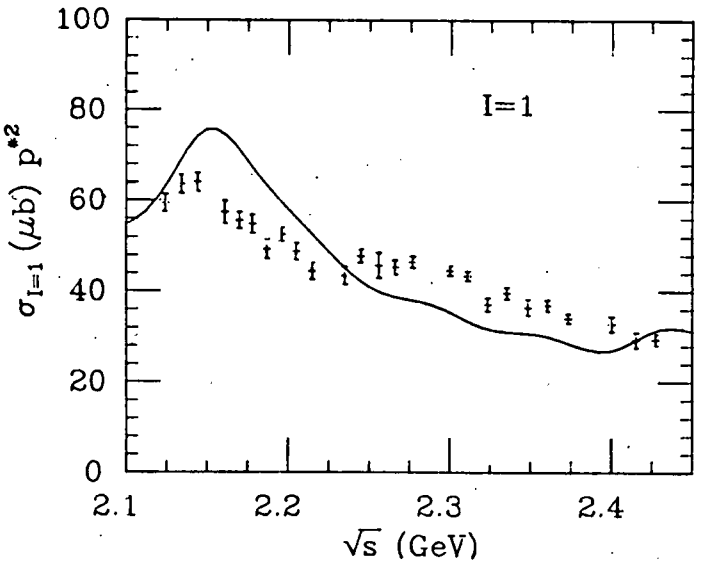

Fig. 7B

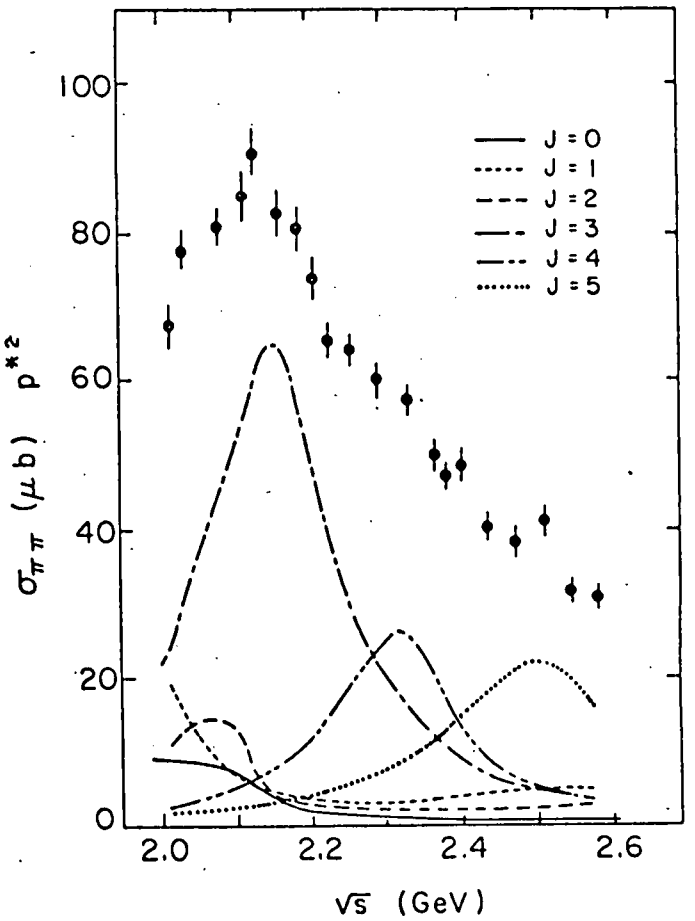

Fig. 8

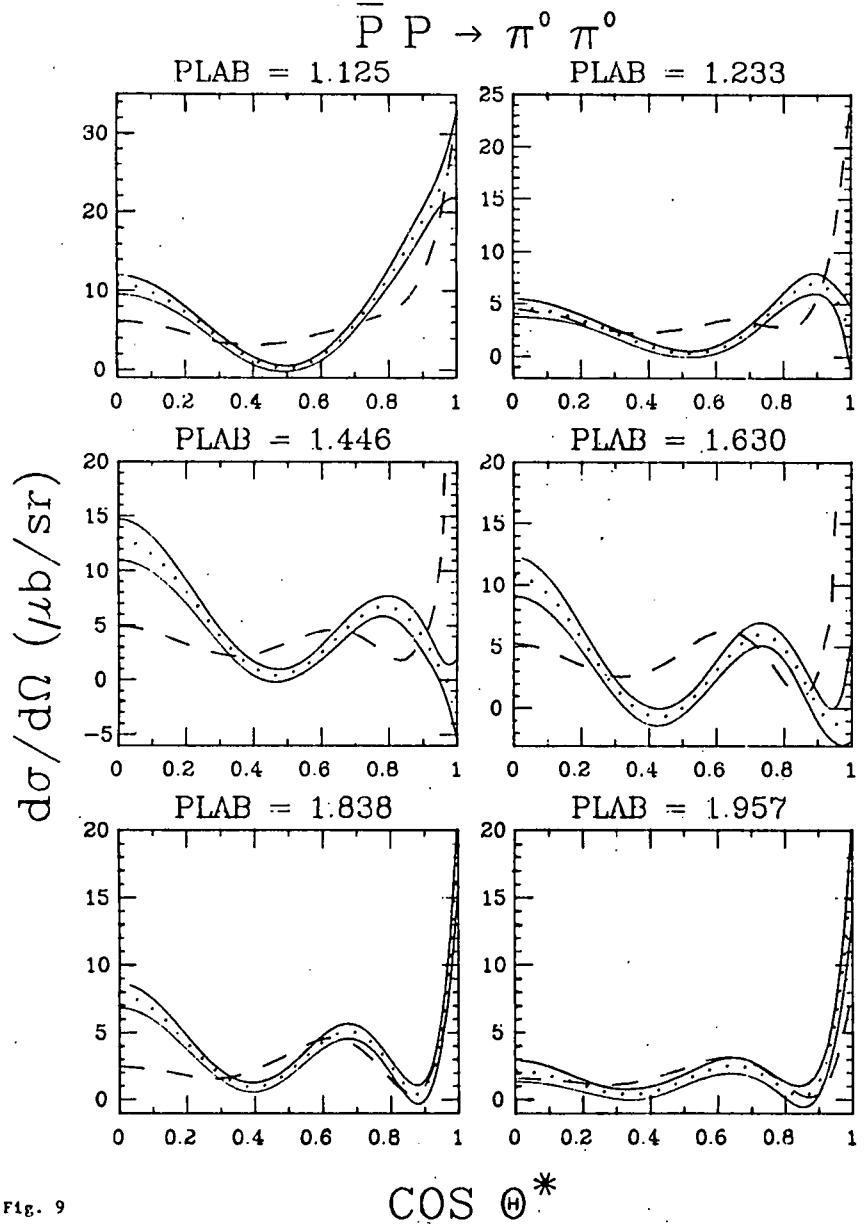
$\bar{P}\,P \rightarrow \pi^0\,\pi^0$
PLAB = 1.125
PLAB = 1.233
PLAB = 1.446
PLAB = 1.630
PLAB = 1.838
PLAB = 1.957
$d\sigma/d\Omega$ (μb/sr)
COS Θ^*

Fig. 9

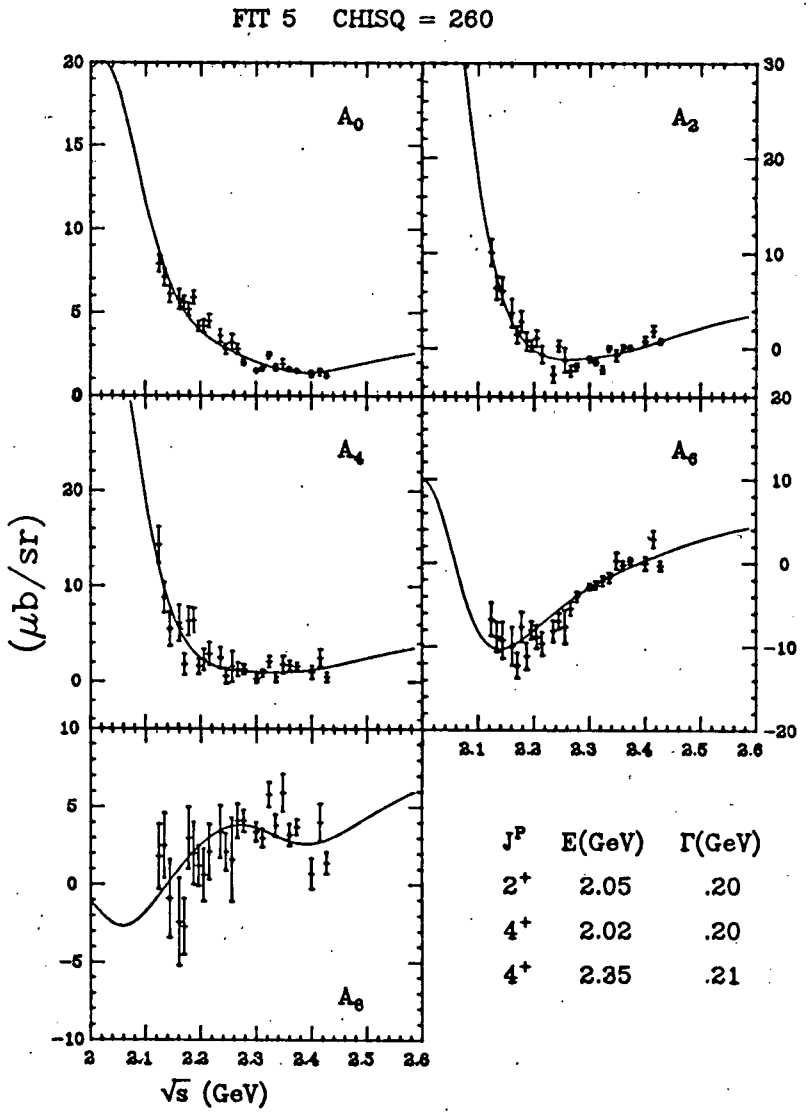
FIT 5 CHISQ = 260
A_0
A_2
A_4
A_6
A_8
(μb/sr)
$\sqrt{s}$ (GeV)
J^P E(GeV) Γ(GeV)
2^+ 2.05 .20
4^+ 2.02 .20
4^+ 2.35 .21

Fig. 10

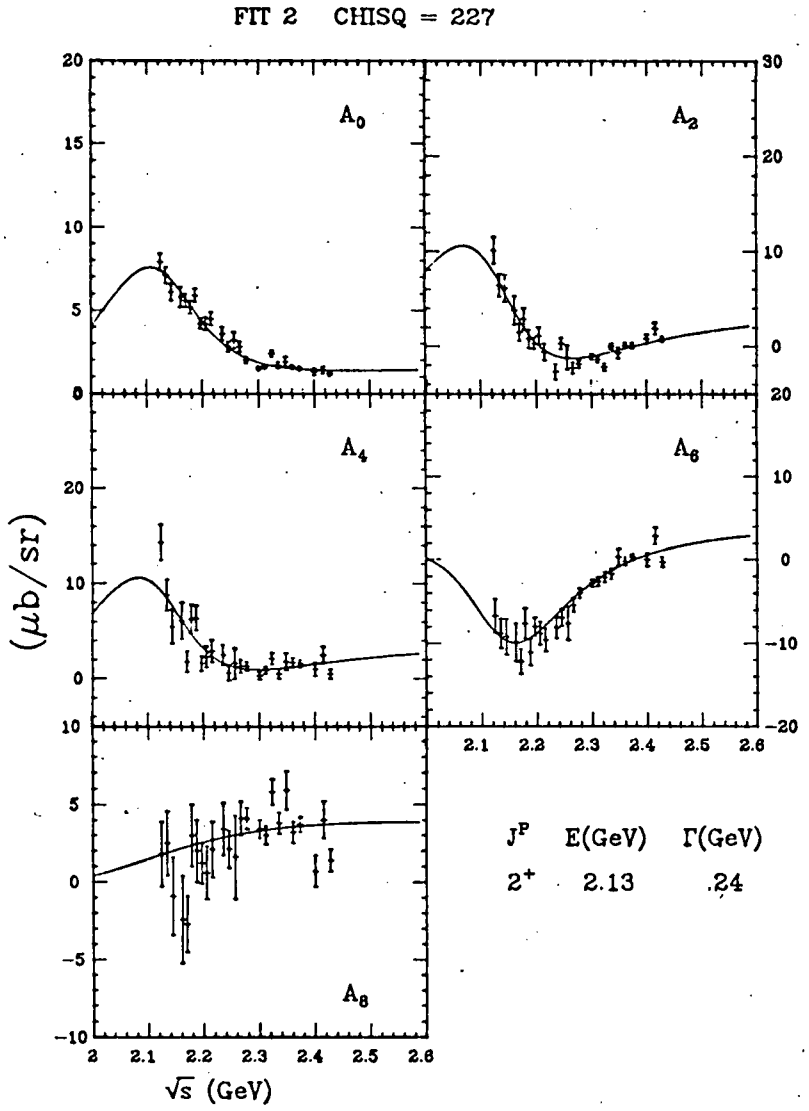

Fig. 11

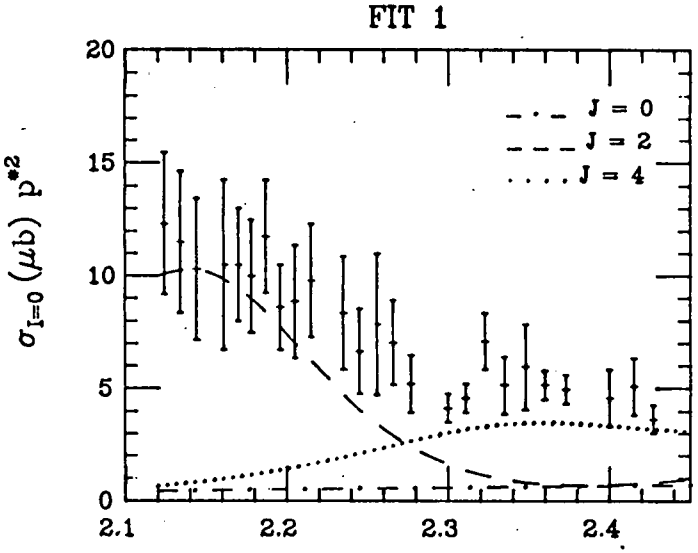

Fig. 12A

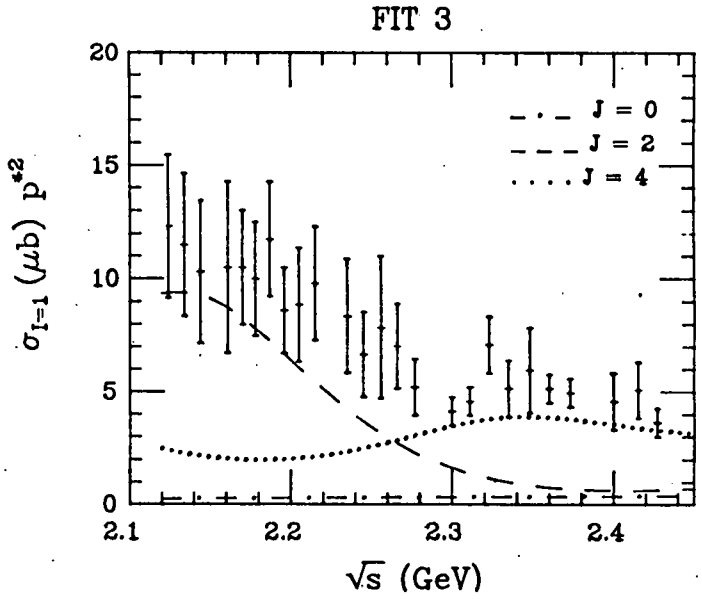

Fig. 12B

CHEW–FRAUTSCHI PLOT

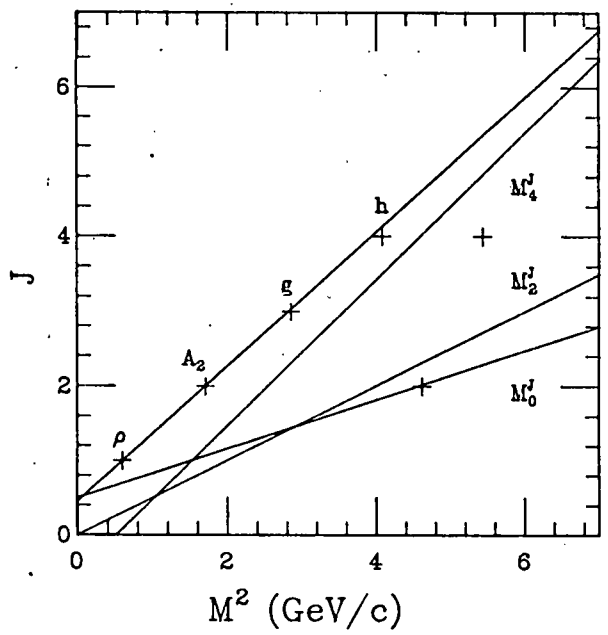

Fig. 13